Research Article | Vol. 27, No. 23 / 11 November 2019 / Optics Express 34093
Optics EXPRESS

Enhanced all-optical cavity-tuning using graphene

ANEESH DASH,[1] UJWOL PALANCHOKE,[2] MARC GELY,[2,3] GUILLAUME JOURDAN,[2,3] SÉBASTIEN HENTZ,[2,3] S. K. SELVARAJA,[1] AND A. K. NAIK[1,*]

[1] *Centre for Nano Science and Engineering, Indian Institute of Science, Bangalore-560012, India*
[2] *CEA, LETI, MINATEC Campus, Grenoble F-38054, France*
[3] *University Grenoble Alpes, Grenoble F-38000, France*
[*] *anaik@iisc.ac.in*

Abstract: All-optical tuning of the resonance of an optical cavity is used to realise optical signal-processing including modulation, switching, and signal-routing. The tuning of optical resonance is dictated by the two primary effects induced by optical absorption: charge-carrier-generation and heat-generation. Since these two effects shift the resonance in opposite directions in a pure silicon-on-insulator (SOI) micro-ring resonator as well as in a graphene-on-SOI system, the efficiency and the dynamic range of all-optical resonance-tuning is limited. In this work, in a graphene-oxide-silicon waveguide system, we demonstrate an exceptional resonance-tuning-efficiency of 300 pm/mW (0.055 π/mW), with a large dynamic range of 1.2 nm (0.22 π) from linear resonance to optical bistability. The dynamics of the resonance-tuning indicates that the superior resonance-tuning is due to large linear-absorption-induced thermo-optic effect. Competing free-carrier dispersion is suppressed as a result of the large separation between graphene and the silicon core. This work reveals new ways to improve the performance of graphene-on-waveguide systems in all-optical cavity-tuning, low-frequency all-optical modulation, and switching.

1. Introduction

All-optical control over optical cavities has been studied for optical transport as well as for applications in optical signal-processing and optical memory [1–3]. In these systems, the intensity of the optical signal is used to modulate the resonant wavelength of the cavity. The third order optical nonlinearity in silicon leads to two-photon absorption (TPA) [3]. TPA generates free carriers and heat in the silicon optical cavity. The heat produces a positive change in the refractive index of silicon and causes a red-shift (shift to longer wavelength) of the cavity-resonance due to the thermo-optic effect in silicon [4]. TPA-generated free carriers cause a negative change in the refractive index of silicon, leading to a blue-shift (shift to shorter wavelength) in the cavity-resonance [3,5]. The competition between the thermo-optic effect and free-carrier dispersion leads to bistability in the transmission response of the optical cavity. Thus the dynamic range of the cavity-tuning before the onset of bistability is limited by TPA. Suppression of the free-carrier effects in a silicon cavity, by depletion of the TPA-generated free carriers, is one way to increase the dynamic range [5]. However, this method involves challenges associated with fabrication. Material platforms like silicon nitride, that don't have TPA, are useful for all-optical cavity-tuning. However, the low thermo-optic effect in silicon nitride makes thermal tuning inefficient. Enhancing the cavity-tuning requires inclusion of other materials on these platforms.

Graphene has been a material of interest in integrated-optic platforms operating at near-infrared (near-IR) wavelengths due to its unique dispersive and dissipative interactions at these wavelengths [6,7]. These interactions have been utilized for electro-optic modulation and resonance-tuning [8,9]. Novel graphene-based sensing platforms are also being developed on integrated-optic platforms [10–12]. Graphene-on-waveguide systems have shown promise for all-optical tuning

#369108 https://doi.org/10.1364/OE.27.034093
Journal © 2019 Received 4 Jun 2019; revised 9 Sep 2019; accepted 10 Sep 2019; published 7 Nov 2019

Optics EXPRESS

and modulation of the spectral response of wavelength-selective devices [13–15]. This is due to the thermo-optic effect caused by large optical absorption in graphene. The tunability of optical absorption in graphene makes it an interesting material for this application. When graphene is integrated over an optical cavity, the thermo-optic effect is significantly enhanced [16]. Such a system is useful for all-optical tuning of the cavity-resonance. However, enhanced TPA in graphene leads to optical bistability, thus limiting the dynamic range of the cavity-tuning [13,14,17–19].

Graphene-on-SiN systems have been shown to have a more efficient all-optical cavity-tuning than pure silicon or SiN systems [13,14]. However, in these experiments, graphene is placed directly over the waveguide and hence, interacts with a strong field. Thus, the TPA in graphene starts at moderate optical powers and the dynamic range from the linear resonance to bistability is low. The bistability induced by the competition between TPA-generated thermo-optic effect and free-carriers in graphene has also been experimentally observed in such geometries [19].

In this work, we show that a silicon dioxide spacer between graphene and the waveguide reduces the strength of the field interacting with graphene, thus reducing the TPA in graphene. As a result, we observe enhanced all-optical tuning of the cavity-resonance, with a large dynamic range of 1.2 nm (0.22 π). We demonstrate all-optical cavity tuning using graphene with an efficiency of 300 pm/mW (0.055 π/mW). We use under-coupled silicon micro-ring resonators, with graphene at a separation of 100 nm from the waveguide. Optical pump-probe measurements are used to determine the response-time of all-optical modulation. The modulation-bandwidth is found to be 3 MHz, indicating that the modulation is dominated by the thermo-optic effect. Time-domain spectral evolution is used for studying the carrier dynamics in silicon micro-ring resonators with and without graphene to investigate the reason behind the enhanced thermo-optic effect. We find that at low power levels, the resonator with graphene exhibits only thermo-optic effect due to cavity-enhanced linear absorption, while no such effect is observed without graphene [16]. The effect of TPA-generated carriers is not observable in both the systems at low optical power. At higher power levels, both thermo-optic effect and carrier-induced effects are observed to be competing in the resonator without graphene. On the other hand, in the resonator with graphene, both linear absorption and TPA make the thermo-optic effect stronger than the carrier-induced effects. Such a system with dominant thermo-optic effect is useful for all-optical cavity-tuning with a large dynamic range.

2. All-optical cavity-tuning

Racetrack micro-ring resonators using single-mode silicon-on-insulator (SOI) waveguides supporting the fundamental quasi-TE mode around 1550 nm wavelength are fabricated using deep-UV lithography followed by reactive-ion-etching. The cross-section of the waveguide is 500 $nm \times 220$ nm. The circumference of the micro-ring is 52 μm and bend-radius is 5 μm. The power coupling coefficient from the straight bus waveguide to the micro-ring resonator is estimated to be approximately 0.4 %. Mechanically exfoliated few-layer graphene flakes are transferred onto the micro-ring resonators. The optical micrograph of the device with graphene is shown in Fig. 1(a). The device with graphene has 3 nm thick graphene covering 7 μm (14 %) of the circumference of the micro-ring. The spectra with and without graphene are shown in Figs. 1(b) and 1(c) respectively. Similar spectra for a pair of other devices with and without graphene (1 nm thick covering 10 % of the micro-ring) can be found in the appendix.

All the input powers referred to herein are at the bus waveguide before being coupled into the micro-ring resonator. It is observed that the device without graphene shows a thermo-optic red shift of 20 pm with increase in optical input power from -8.1 dBm to 6.6 dBm at the straight waveguide. However, the device with graphene shows an extra-ordinary red-shift of 1.2 nm with increase in optical input power from -4.8 dBm to 6.6 dBm at the straight waveguide. Similar observations have been previously reported using monolayer graphene on Silicon-Nitride

Optics EXPRESS

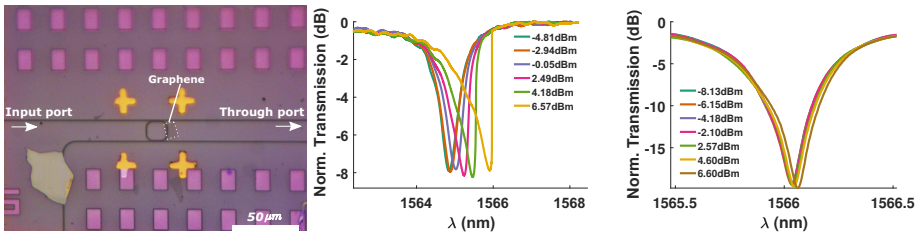

Fig. 1. (a) Optical micrograph of the micro-ring resonator with graphene, (b) All-optical tuning in a micro-ring resonator with multi-layer graphene (3 *nm* thick) covering 14 % of the circumference: a large tuning-efficiency (red-shift) of 300 pm/mW (0.055 π/mW) and linear dynamic range of 1.2 *nm* (0.22 π) are observed, (c) All-optical tuning in a micro-ring resonator without graphene: a low red-shift of 20 *pm* for 4 *mW* optical power is observed.

micro-ring resonators and have been attributed to the thermo-optic effect in graphene at high optical powers [14]. However, it must be noted that the overall red shift from the cold-cavity resonance to the onset of bistability in our case is 1.2 *nm* (0.22 π) and the tuning-efficiency is 300 pm/mW (0.055 π/mW). These values are much larger than the previously reported values [14]. A comparison between the all-optical cavity-tuning observed in our devices and the previously reported values is shown in Table 1. It must be noted that our devices contain few-layer graphene unlike monolayer graphene in the previous reports. However, the gradual reduction of the tuning efficiency from the device with 3 *nm*-thick graphene to the device with 1 *nm*-thick graphene indicates an estimated tuning-efficiency of the order of 100 pm/mW for monolayer graphene, that is better than the previous reports. We investigate the reason behind this large tuning-efficiency and high dynamic range in this article.

Table 1. Comparison of All-optical Cavity-tuning using Graphene-oxide-SOI MRR with Graphene-SiN MRR Systems

MRR System\Parameter	Thick-ness (nm)	Cover-age (%)	Tuning-efficiency (pm/mW)	Dynamic Range (nm)
Graphene-SiN [14]	0.34	20	23	0.4
Graphene-SiN [13]	0.34	23	8(0.003 π)	–
Graphene-Oxide-SOI [this work]	3	14	300(0.055 π)	1.2(0.22 π)
Graphene-Oxide-SOI [this work]	1	10	240(0.044 π)	$\geq$ 0.5(0.09 π)

The results in Fig. 1(b) were obtained by a slow wavelength-sweep of a tunable continuous-wave (CW) laser source. The transmitted power was recorded at a wavelength-step of 1 *pm* and a hold-time of 20 μs, that is expected to be larger than the life-time of the thermo-optic effect. Thus the effect of the carrier-generation at all values of detuning from the resonance was observed. To observe the thermo-optic shift at a fixed detuning from the cold-cavity resonance, we use a broadband probe laser at the input to monitor the change in the spectrum at different pump powers. The output of the device from the through-port of the resonator is observed in an optical spectrum analyzer.

Two consecutive resonances of the device, around 1555 *nm* and 1565.25 *nm*, are monitored. The results are shown in Figs. 2(a) and 2(b). The wavelength of the pump laser is set to be around the resonance at 1565.25 *nm*. We perform all-optical cavity-tuning with a pump that is initially blue-detuned (shorter wavelength) from the resonance by 0.5 *nm*. The effect of the tuning is observed by monitoring the broadband probe around the resonance at 1555 *nm*. We observe that the cavity-tuning is 0.4 *nm* for a change in the pump power from 0 *dBm* to 5 *dBm*. As expected,

Optics EXPRESS

the tuning is lower than that in Fig. 1(b) due to the large detuning of the pump from the resonance. Also, no asymmetry in the resonance around 1555 *nm* is observed at these power levels. Similar measurements carried out on micro-ring resonators without graphene do not exhibit any shift in the resonance.

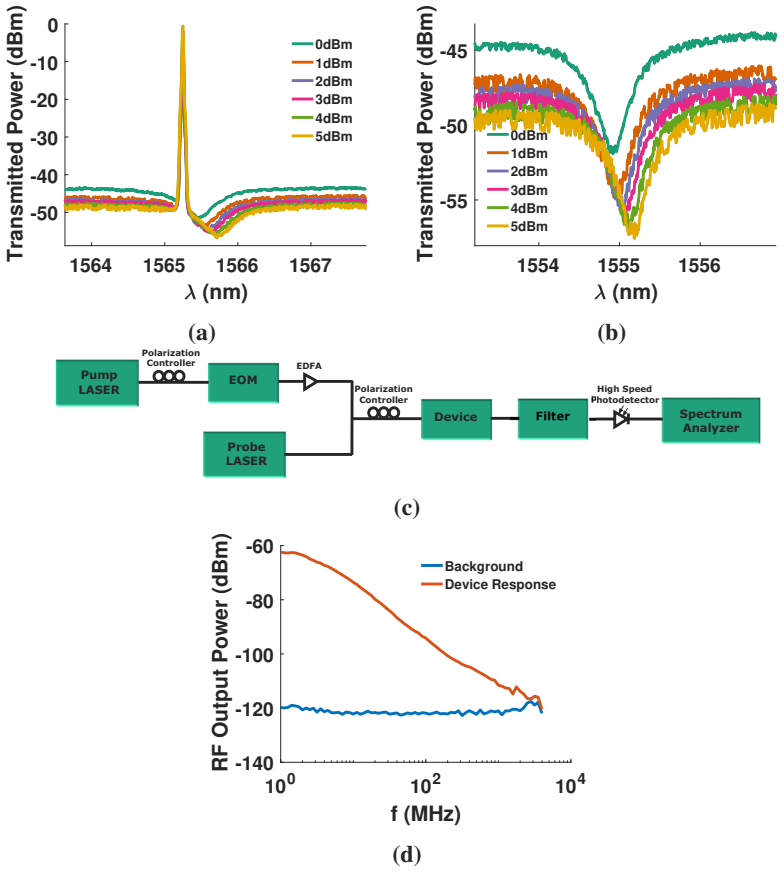

Fig. 2. (a) Single-wavelength CW pump at a blue detuning of 0.4 *nm* from the cold-cavity resonance: increase in the pump power cause the resonance to red-shift by 100 pm/mW for the device with graphene due to the thermo-optic effect, (b) The corresponding cavity tuning is observed at a consecutive resonance with a broadband probe, (c) Measurement-schematic for all-optical modulation of a CW probe laser with a sinusoidally intensity-modulated pump, (d) Frequency response of the all-optical modulation: a 3 *dB* cut-off frequency of 3 *MHz* is observed indicating that the modulation is dominated by the thermo-optic effect.

This consistent red-shift in the resonance undoubtedly indicates the dominance of the thermo-optic effect for a CW input. The change in the spectrum, with the intensity of the pump indicates all-optical modulation. To determine the bandwidth of the all-optical modulation, we replace the continuous-wave pump with an intensity-modulated pump and the broad-band probe with a single-wavelength CW laser. The probe input is set at the blue-detuned slope of the resonance close to 1555 *nm*. The schematic for the measurement is shown in Fig. 2(c). At the output of the device, the pump is filtered out using an optical band-pass filter around the wavelength of the probe laser. The optical output is passed into a high-frequency photo-detector and the corresponding electrical output of the photo-detector is given as an input into the spectrum analyzer. The result of the measurement is shown in Fig. 2(d). The modulation of the pump

Optics EXPRESS

power causes modulation of the resonance of the micro-ring resonator. The power of probe laser, that is at the slope of the resonance, gets modulated at the same frequency. The 3 *dB* cut-off frequency of the modulated output in Fig. 2(d) is around 3 *MHz*. This response-time ($\approx$ 330 *ns*) is characteristic of the thermo-optic effect [13].

3. Dynamics of cavity-tuning

To study the transient all-optical response of the device, we use a pulsed laser as the pump. The probe laser is not used in this measurement. The measurement schematic is shown in Fig. 3(a). We use pulses of 1 μs on-time and 19 μs off-time. The on-state power levels used for these measurements are significantly larger than the CW powers used in Figs. 1(b) and 1(c) respectively, since the detuning from the cold-cavity resonance is large. The output at the through-port of the micro-ring resonator is passed into a high frequency photo-detector. We set the input laser at an initial red-detuning of 0.4 *nm* from the resonance. Similar measurements are also performed on a device without graphene. The dynamic tuning of the resonance results in a dynamic change of the detuning of the optical input from the resonance, as depicted in the left inset of Fig. 3(a). The normalized results of the measurements on the resonators with and without graphene, for a series of increasing input powers, are shown in Figs. 3(b) and 3(c) respectively.

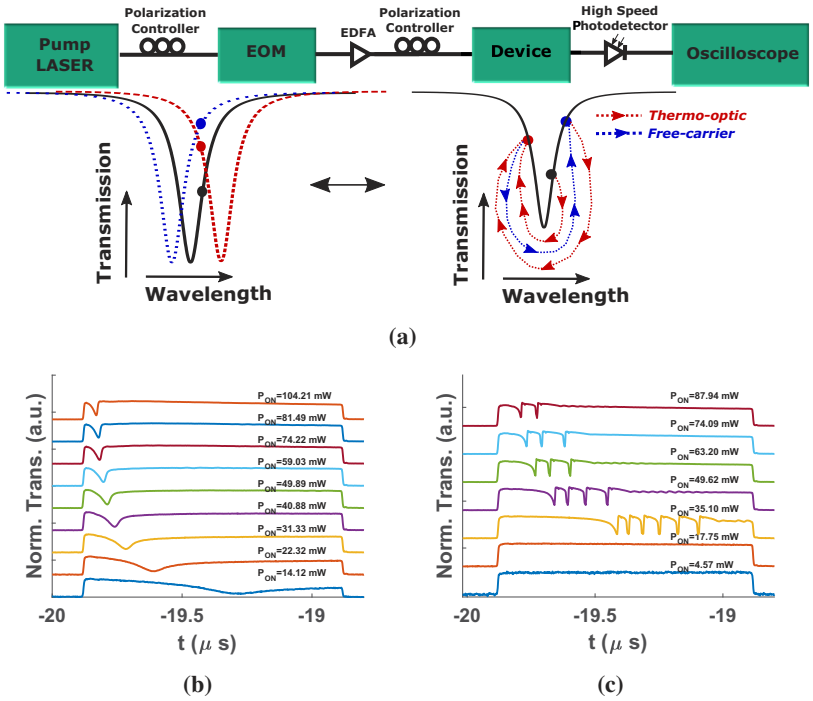

Fig. 3. (a) Measurement-schematic for acquiring time-domain transient response with a high power pulse-modulated pump laser; the insets depict the dynamic tuning of the resonance and the time-varying detuning of the pump from the resonance due to red-shift caused by thermo-optic effect or blue-shift caused by free-carrier dispersion , (b) Time domain response of the device with graphene for 1 μs pulses at different on-state optical powers: at low powers, cavity-enhanced linear absorption in graphene causes red-shift in the resonance, producing a dip in the time trace and at higher powers, the thermo-optic effect becomes stronger the transition becomes sharper, (c) Competition between thermo-optic effect and free carriers is observed in the resonator without graphene at higher optical powers: this is due to TPA; no effect of carriers is observable at lower powers.

Optics EXPRESS

For input powers starting from 14 mW upto 104 mW, the output response of the device with graphene has a fall and a subsequent rise with time. This can be understood as the transition depicted using red arrows in the right inset of Fig. 3(a). The initial red-detuned (longer wavelength) input in the on-state, marked by a black circle, initiates the thermo-optic effect in the micro-ring resonator. The thermo-optic effect causes the overall index of the micro-ring resonator to increase, thereby producing a red-shift in the resonance. If the red-shift is large enough for the resonant wavelength to cross the input wavelength, the input is now blue-detuned from the resonance, depicted by a red circle. The power of the input is fixed during this transition. Hence, the fall in the output power is attributed to the dynamic change in detuning from the resonance and the minimum output power is the instant when the input is at the resonance. During this process, the detuning of the pump laser from the resonance changes dynamically and depending on the power, the thermo-optic effect may be caused by linear absorption, TPA, or both. We operate at power levels far below the threshold for saturable absorption in graphene [20]. Hence, the free-carriers, if generated, are primarily due to TPA.

The time-trace of the output signal from the device without graphene has multiple sets of fall and rise for input powers $\geq 35\ mW$, while no such dips are observed at lower powers. The first dip in the time trace is due to the thermo-optic effect, similar to the resonator with graphene. This transition can be understood by the red arrow in the right inset of Fig. 3(a). After the first dip, the pump is blue-detuned from the resonance, as shown with a red circle in the inset of Fig. 3(a). In this state, if the density of the TPA-generated free carriers is sufficient to produce a blue-shift that compensates for the thermo-optic red-shift, the resonance starts to experience a net blue-shift. If the blue-shift is large enough, the density of the free carriers reduces and the input again comes to a red-detuned state (blue circle) due to the thermo-optic effect. This transition is depicted using blue arrows in the right inset of Fig. 3(a). Thus, the competition between the thermo-optic effect and the free carriers produces multiple dips in Fig. 3(c) for the device without graphene. This competition starts at higher powers, further indicating that the origin of the free-carriers is from TPA. This phenomenon has been extensively studied in optical cavities made of silicon [1,2]. However, in the device with graphene we do not observe any such competition and the thermo-optic effect dominates, even for input powers as high as 104 mW.

We then perform the same experiment at multiple values of the initial detuning from the cold-cavity resonance. The results for an input power of around 100 mW for the devices with and without graphene are shown in Figs. 4(a) and 4(b) respectively. The observations in the two resonators remains unchanged when the pump is initially red-detuned from the cold-cavity resonance. In the last trace in Figs. 4(a) and 4(b), the pump is set at a large initial blue detuning from the cold-cavity resonance. Since the density of free carriers is insufficient to produce a large blue shift of the resonance in either case, no crossing of the resonance is observed. The extended set of data at different combinations of power and wavelength of the pump can be found in the appendix.

To qualitatively analyze the dynamic density of carriers in both these devices, we follow the theoretical framework used for similar measurements with silicon optical cavities [1,2]. The dynamic loss-rate in the micro-ring resonator, that affects the dynamic resonance-tuning, is given as [2]

$$\gamma(t) = f_{TPA}|a(t)|^2 + f_{FCA}N(t) + \gamma_l\,, \tag{1}$$

where $a(t)$ and $N(t)$ are the time-varying mode-amplitude and free-carrier density respectively, f_{FCA} is the free-carrier absorption coefficient, γ_l is the linear absorption rate in the cavity, and f_{TPA} is the TPA-coefficient [2].

The Q-factors of the micro-ring resonators with and without graphene are 2500 and 5200 respectively. The TPA coefficient (f_{TPA}) is larger for a silicon waveguide with graphene in direct contact than for an ordinary silicon waveguide [19]. However, the graphene in our device is 100 nm above the waveguide, separated by an oxide spacer. For such a sytem, the TPA is expected

Optics EXPRESS

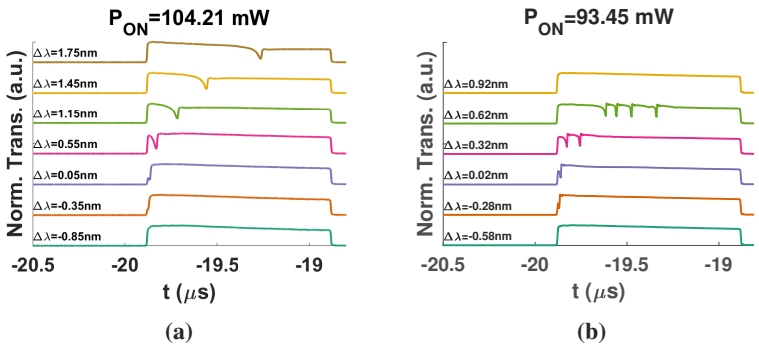

Fig. 4. Wavelength dependence of the carrier dynamics in resonators (a) with graphene and (b) without graphene respectively: The resonator with graphene exhibits dominance of the thermo-optic effect, while the one without graphene shows competition between free carriers and the thermo-optic effect.

to be almost the same as a silicon waveguide without graphene. We find this to be true using numerical simulations in a finite-element model using the cross-section shown in Fig. 5(a). The coverage of graphene is assumed to be 100 %. The results are shown in Fig. 5(b). The TPA due to graphene is further reduced by maintaining a partial coverage over the micro-ring ($\leq$ 14% in our case). On the other hand, the linear absorption rate γ_l is significantly larger for the device with graphene than the one without graphene, even with the 100 *nm* oxide spacer; the computed values of propagation loss shown in Fig. 5(c). Free-carrier generation is dependent on TPA (for the power levels used in our experiments), while thermo-optic effect is dependent on both linear absorption and TPA. Hence, the relative strength of the thermo-optic effect is expected to be larger than the free-carrier dispersion (dependent on TPA) in the micro-ring with graphene. Thus, the higher linear absorption in presence of graphene enhances the thermo-optic effect at low powers (even at large detuning from the resonance), as is evident from Fig. 3(b) for $P_{ON} \leq 35\ mW$. On the contrary, the resonator without graphene, shows no observable cavity-tuning at similar power levels, as shown in Fig. 3(c).

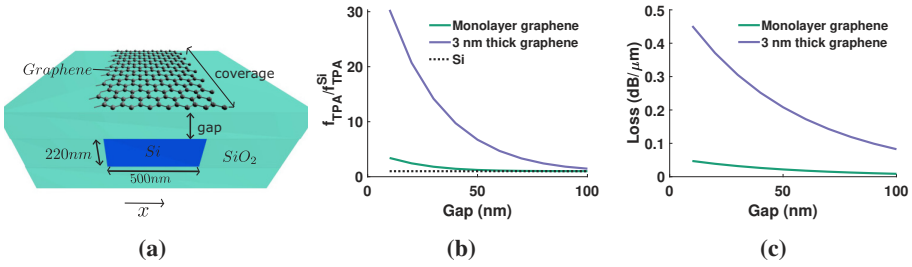

Fig. 5. (a) Cross-section of the SOI waveguide with graphene: the gap between the waveguide and graphene is filled with silicon dioxide, (b) Variation of the normalized TPA-coefficients of a SOI waveguide, with monolayer and 3 *nm* thick graphene, with change in the oxide-filled gap, (c) Variation of the additional propagation loss due to graphene in the waveguide-systems: At a gap of 100 *nm*, the TPA-coefficient of the SOI waveguide with 3 *nm* thick graphene is almost the same as that without graphene, but the propagation loss is significantly larger.

At higher powers ($P_{ON} \geq 35\ mW$), multiple dips are observed in the response of the resonator without graphene, as seen in Fig. 3(c). We identify this as the onset of TPA in the resonator

Optics EXPRESS

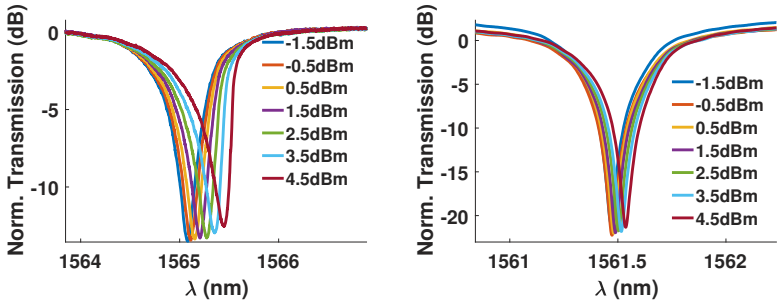

Fig. 6. (a) All-optical tuning in a micro-ring resonator with multi-layer graphene (1 *nm* thick) covering 10 % of the circumference of the micro-ring: a large tuning-efficiency (red-shift) of 240 pm/mW and linear dynamic range of $\geq$ 0.5 *nm* are observed, (b) All-optical tuning in another micro-ring resonator without graphene.

without graphene. The optical power for the onset of TPA in the resonator with graphene can be expected to be double, since the Q-factor is half that of the resonator without graphene. Even at higher optical powers, only a single dip is observed in the response of the device with graphene. Thus, the thermo-optic effect dominates over the free carriers in the resonator with graphene. This is the reason behind the large dynamic range and tuning-efficiency of all-optical cavity-tuning in presence of graphene.

4. Conclusion

In conclusion, we have demonstrated enhanced all-optical cavity-tuning in an under-coupled silicon micro-ring resonator in presence of multilayer graphene covering $\leq$ 14 % of the micro-ring resonator. The resonator shows a tuning of 300 pm/mW (0.055 π/mW), dominated by the thermo-optic effect and an overall dynamic range of 1.2 *nm* (0.22 π) from linear resonance to bistability. On the contrary, a similar micro-ring resonator without graphene is shown to have negligible tuning for the same power levels. The reason behind the superior resonance-tuning of the micro-ring resonator with graphene has been investigated. All-optical pump-probe modulation and the dynamics of all-optical resonance-tuning with an optical pump indicate dominant thermo-optic effect even at high optical powers. Numerical estimates of the variation of linear absorption and TPA, with separation between graphene and the silicon core, indicate that at a separation of 100 *nm*, the additional contribution of TPA in graphene to the TPA in silicon is minimal and the linear absorption dominates. Hence, red-shift of the resonance due to linear-absorption-induced thermo-optic effect outweighs the blue-shift due to TPA-induced free-carrier dispersion. Therefore, enhanced all-optical cavity-tuning is observed in the graphene-oxide-silicon waveguide system. This device-configuration is useful for applications in controlled low frequency all-optical modulation and switching.

Appendix A. Cavity tuning on a second pair of devices with and without graphene

The results of all-optical cavity tuning for a second pair of devices with and without graphene is shown in Fig. 6. The graphene flake is 1 *nm* thick and covers 10 % of the circumference of the micro-ring resonator. A tuning-efficiency of 240 pm/mW and linear dynamic range of $\geq$ 0.5 *nm* are observed for the device with graphene.

Optics EXPRESS

Appendix B. Extended data: time-domain measurements with a pulse-modulated pump on devices with and without graphene

The extended data for time-domain measurements on the pair of devices with and without graphene is shown in Fig. 7. The device without graphene shows competition between thermo-optic effect and free-carrier dispersion, while the one with graphene shows dominant thermo-optic effect.

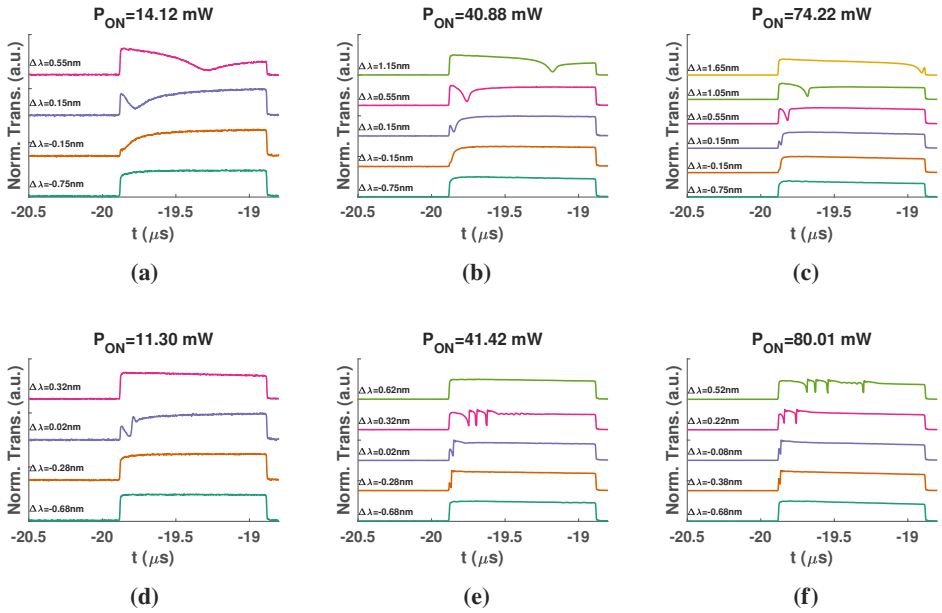

Fig. 7. Wavelength and power dependence of the carrier dynamics in resonators (a)-(c) with and (d)-(f) without graphene: The resonator with graphene shows dominant thermo-optic effect, while competition between thermo-optic effect and free-carrier dispersion are observed in the resonator without graphene (in traces with multiple dips).

Funding

Council of Scientific and Industrial Research, India; Department of Science and Technology, Ministry of Science and Technology (Nano Mission SR/NMITP-62/2016(G)); Ministry of Human Resource Development; Ministry of Electronics and Information Technology and Department of Science and Technology (NNetRA).

Acknowledgments

We thank Ms. Vadivukkarasi Jeyaselvan and Ms. Roopa Prakash for their assistance in some experimental trials, and Dr. V. R. Supradeepa for helpful technical discussions.

References

1. W. H. P. Pernice, M. Li, and H. X. Tang, "Time-domain measurement of optical transport in silicon micro-ring resonators," Opt. Express **18**(17), 18438–18452 (2010).
2. T. J. Johnson, M. Borselli, and O. Painter, "Self-induced optical modulation of the transmission through a high-Q silicon microdisk resonator," Opt. Express **14**(2), 817–831 (2006).
3. J. Leuthold, C. Koos, and W. Freude, "Nonlinear silicon photonics," Nat. Photonics **4**(8), 535–544 (2010).
4. A. Dash, V. Mere, P. R. Y. Gangavarapu, S. R. Nambiar, S. K. Selvaraja, and A. K. Naik, "Carbon-nanotube-on-waveguide thermo-optic tuners," Opt. Lett. **43**(21), 5194–5197 (2018).
5. M. Sodagar, M. Miri, A. A. Eftekhar, and A. Adibi, "Optical bistability in a one-dimensional photonic crystal resonator using a reverse-biased pn-junction," Opt. Express **23**(3), 2676–2685 (2015).

Optics EXPRESS

6. G. W. Hanson, "Dyadic Green's functions and guided surface waves for a surface conductivity model of graphene," J. Appl. Phys. **103**(6), 064302 (2008).
7. V. Sorianello, G. D. Angelis, T. Cassese, M. Midrio, M. Romagnoli, M. Mohsin, M. Otto, D. Neumaier, I. Asselberghs, J. V. Campenhout, and C. Huyghebaert, "Complex effective index in graphene-silicon waveguides," Opt. Express **24**(26), 29984–29993 (2016).
8. Y. Ding, X. Zhu, S. Xiao, H. Hu, L. H. Frandsen, N. A. Mortensen, and K. Yvind, "Effective electro-optical modulation with high extinction ratio by a graphene-silicon microring resonator," Nano Lett. **15**(7), 4393–4400 (2015). ArXiv: 1502.00480.
9. C. T. Phare, Y.-H. Daniel Lee, J. Cardenas, and M. Lipson, "Graphene electro-optic modulator with 30 GHz bandwidth," Nat. Photonics **9**(8), 511–514 (2015).
10. C.-H. Liu, Y.-C. Chang, T. B. Norris, and Z. Zhong, "Graphene photodetectors with ultra-broadband and high responsivity at room temperature," Nat. Nanotechnol. **9**(4), 273–278 (2014).
11. Z. Cheng and K. Goda, "Design of waveguide-integrated graphene devices for photonic gas sensing," Nanotechnology **27**(50), 505206 (2016).
12. A. Dash, S. K. Selvaraja, and A. K. Naik, "On-chip optical transduction scheme for graphene nano-electro-mechanical systems in silicon-photonic platform," Opt. Lett. **43**(4), 659–662 (2018).
13. C. Qiu, Y. Yang, C. Li, Y. Wang, K. Wu, and J. Chen, "All-optical control of light on a graphene-on-silicon nitride chip using thermo-optic effect," Sci. Rep. **7**(1), 17046 (2017).
14. Y. Gao, W. Zhou, X. Sun, H. K. Tsang, and C. Shu, "Cavity-enhanced thermo-optic bistability and hysteresis in a graphene-on-Si_3N_4 ring resonator," Opt. Lett. **42**(10), 1950–1953 (2017).
15. Z. Sun, A. Martinez, and F. Wang, "Optical modulators with 2D layered materials," Nat. Photonics **10**(4), 227–238 (2016).
16. H. Cai, Y. Cheng, H. Zhang, Q. Huang, J. Xia, R. Barille, and Y. Wang, "Enhanced linear absorption coefficient of in-plane monolayer graphene on a silicon microring resonator," Opt. Express **24**(21), 24105–24116 (2016).
17. K. Alexander, N. A. Savostianova, S. A. Mikhailov, B. Kuyken, and D. V. Thourhout, "Electrically Tunable Optical Nonlinearities in Graphene-Covered SiN Waveguides Characterized by Four-Wave Mixing," ACS Photonics **4**(12), 3039–3044 (2017).
18. B. Yao, S.-W. Huang, Y. Liu, A. K. Vinod, C. Choi, M. Hoff, Y. Li, M. Yu, Z. Feng, D.-L. Kwong, Y. Huang, Y. Rao, X. Duan, and C. W. Wong, "Gate-tunable frequency combs in graphene-nitride microresonators," Nature **558**(7710), 410–414 (2018).
19. T. Gu, N. Petrone, J. F. McMillan, A. v. d. Zande, M. Yu, G. Q. Lo, D. L. Kwong, J. Hone, and C. W. Wong, "Regenerative oscillation and four-wave mixing in graphene optoelectronics," Nat. Photonics **6**(8), 554–559 (2012).
20. A. Marini, J. D. Cox, and F. J. Garcia de Abajo, "Theory of graphene saturable absorption," Phys. Rev. B **95**(12), 125408 (2017).